Geomechanics and Engineering, *Vol. 14, No. 6 (2018) 589-600*
DOI: https://doi.org/10.12989/gae.2018.14.6.589

Stochastic analysis for uncertain deformation of foundations in permafrost regions

Tao Wang*, Guoqing Zhou, Jianzhou Wang, Xiaodong Zhao and Leijian Yin

State Key Laboratory for Geomechanics and Deep Underground Engineering, School of Mechanics and Civil Engineering, China University of Mining and Technology, Xuzhou, Jiangsu, 221116, China

(Received August 23, 2016, Revised September 7, 2017, Accepted November 7, 2017)

Abstract. For foundations in permafrost regions, the displacement characteristics are uncertain because of the randomness of temperature characteristics and mechanical parameters, which make the structural system have an unexpected deviation and unpredictability. It will affect the safety of design and construction. In this paper, we consider the randomness of temperature characteristics and mechanical parameters. A stochastic analysis model for the uncertain displacement characteristic of foundations is presented, and the stochastic coupling program is compiled by Matrix Laboratory (MATLAB) software. The stochastic displacement fields of an embankment in a permafrost region are obtained and analyzed by Neumann stochastic finite element method (NSFEM). The results provide a new way to predict the deformation characteristics of foundations in permafrost regions, and it shows that the stochastic temperature has a different influence on the stochastic lateral displacement and vertical displacement. Construction disturbance and climate warming lead to three different stages for the mean settlement of characteristic points. For the stochastic settlement characteristic, the standard deviation increases with time, which imply that the results of conventional deterministic analysis may be far from the true value. These results can improve our understanding of the stochastic deformation fields of embankments and provide a theoretical basis for engineering reliability analysis and design in permafrost regions.

Keywords: stochastic analysis; uncertain deformation; foundations; permafrost regions; random field

1. Introduction

During the operation of Qinghai-Tibet Railway, the embankment and its underlain permafrost are affected by global warming, which will accelerate the changes of thermal state in the frozen foundation. And the temperature change will lead to a series of mechanical behavior variations of frozen soil (Ma and Wang 2014). Usually, these variations are very complex and they will have a direct effect on the stability of the embankment in permafrost regions. Thus far, many scholars have been trying to solve the problems of foundation deformation and disaster forecasts in permafrost regions. For example, some empirical and semi-empirical formulae were proposed, which are easily used in engineering (Liu *et al*. 2002, Wang, *et al*. 2015, Wang, *et al*. 2016,). Some in-situ tests were carried out to study deformation characteristics of railway and highway embankment in permafrost regions (Yu *et al*. 2002, Sun *et al*. 2003, Li *et al*. 2006, Mohammed *et al*. 2015). Furthermore, finite element method (FEM) was extensively used to analyze the thermal and mechanical stability of frozen embankment because of the advantages of low cost and short research turnaround (Wang *et al*. 2006, Mao *et al*. 2006, Lee, *et al*. 2015). However, all of the researches of deformation characteristic for embankment are always deterministic, rather than taking stochastic temperature and parameters into account.

In fact, the property parameters of soil are variable because of the complex geological processes (Elkateb *et al*. 2003, Dasaka and Zhang 2012, Parinaz and Ehsan 2016, Khemis *et al*. 2016). Especially for permafrost regions, the structure of frozen soil varies with the random distribution of internal defects. Therefore, its mechanics properties exhibit randomness and uncertainty, and the stress-strain relationship, especially of warm frozen soil and warm ice-rich frozen soil, can not be described well deterministically (Lai *et al*. 2008 and 2012). Furthermore, some scholars paid their attention on the stochastic thermal analysis in permafrost regions, and the random temperature fields of railway and highway embankment are obtained by first-order perturbation technique and Neumann stochastic finite element method (Liu *et al*. 2006, 2007, and 2014, Wang *et al*. 2015, Zhou *et al*. 2015). For frozen soil, it is obvious that the randomness of soil temperature will lead to the randomness of mechanical parameters because they are closely related. Therefore, it is extremely significant to consider the stochastic aspects of the temperature and parameters when the stability analysis of displacement characteristics for embankment in permafrost regions is to be conducted.

In this paper, at first, a stochastic analysis model of deformation characteristics for foundation in permafrost regions is developed based on theories of elastic-plastic finite element and random field. Afterwards, an embankment of Qinghai-Tibet Railway is taken as an

*Corresponding author, Ph.D.
E-mail: wtbtj@126.com

ISSN: 2005-307X (Print), 2092-6219 (Online)

example, and the stochastic deformation fields are obtained by NSFEM. According to the distributions of mean and standard deviation, the change rules of stochastic deformation fields are analyzed in detail. From this study, some useful conclusions will be drawn, which can provide theoretical basis and reference for design, maintenance and research on the embankment in permafrost regions.

2. Deterministic mathematical equations and finite element formulae

According to the earlier studies of stochastic analysis model for uncertain temperature characteristics for embankment in permafrost regions (Wang *et al.* 2015), we obtained the random temperature fields. This paper focuses on the stochastic deformation of foundations in permafrost regions. Therefore, we will not introduce the calculation process of random temperature fields, repeatedly.

2.1 Governing differential equations

In soil mechanics, the compression is often defined as positive. For a static case, the local equilibrium equation is obtained as a force balance on a small differential volume of deformed frozen soil and is given by (Davis and Selvadurai 2002)

$$[\partial]^{\mathrm{T}}\{\sigma\}-\{f\}=0 \tag{1}$$

where $[\partial]$ denotes the differential operator matrix, and $[\partial]=\begin{bmatrix}\frac{\partial}{\partial x} & 0 & \frac{\partial}{\partial y}\\ 0 & \frac{\partial}{\partial y} & \frac{\partial}{\partial x}\end{bmatrix}^{\mathrm{T}}$; $\{\sigma\}$ is the stress vector, and $\{\sigma\}=\{\sigma_x \quad \sigma_y \quad \tau_{xy}\}^{\mathrm{T}}$; $\{f\}$ is the body force vector, $\{f\}=\{f_x \quad f_y\}^{\mathrm{T}}$.

Based on the assumption that strain is small and compressive strain is assumed positive, the strain-displacement relation of soil can be defined as

$$\{\varepsilon\}=-[\partial]\{u\} \tag{2}$$

where $\{\varepsilon\}$ is the strain vector, and $\{\varepsilon\}=\{\varepsilon_x \quad \varepsilon_y \quad \gamma_{xy}\}^{\mathrm{T}}$; $\{u\}$ is the displacement vector, and $\{u\}=\{u_x \quad u_y\}^{\mathrm{T}}$.

2.2 Boundary conditions and initial conditions

As a general embankment structure, the stress boundary condition and displacement boundary conditions should be satisfied on the boundary. It can be expressed as

$$\{n\}\{\sigma\}=\{\overline{f}\} \tag{3}$$

$$\{u\}=\{\overline{u}\} \tag{4}$$

where $\{n\}$ is the outer normal vector of the boundary; $\{\overline{f}\}$ is the surface force of the boundary, and $\{\overline{f}\}=\{\overline{f_x} \quad \overline{f_y}\}$; $\{\overline{u}\}$ is the displacement of the boundary, and $\{\overline{u}\}=\{\overline{u_x} \quad \overline{u_y}\}$.

For the problem of elastic-plastic analysis, the initial conditions are as follows

$$\{\sigma\}=\{\sigma_0\} \tag{5}$$

$$\{u\}=\{u_0\} \tag{6}$$

where $\{\sigma_0\}$ the initial stress vector; $\{u_0\}$ is the initial displacement vector.

2.3 Stress-strain relationship

According to the constitutive model for clays (Yao *et al*. 2007, 2008 and 2012), Wang (2015) obtained a constitutive model for frozen soil, which took the cohesion into account. The current yield function and reference yield function in the *p*-*q* plane can be written as

$$f=\ln\frac{p}{p_0}+\ln\left(1+\frac{q^2}{M^2p(p+p_r)}\right)-\int\frac{M^4\left(M_f^4-\eta^4\right)}{M_f^4\left(M^4-\eta^4\right)}\frac{d\varepsilon_v^p}{\varphi'(\ln p)-\kappa}=0 \tag{7}$$

$$f=\ln\frac{\overline{p}}{\overline{p}_0}+\ln\left(1+\frac{\overline{q}^2}{M^2\overline{p}(\overline{p}+p_r)}\right)-\int\frac{d\varepsilon_v^p}{\psi'(\ln\overline{p})-\kappa}=0 \tag{8}$$

where p_0 is the spherical stress of current yield surface for the initial condition; $\overline{p}_0$ is the spherical stress of reference yield surface for the initial condition; M is the stress ratio at the critical state in triaxial compression; p_r is a constant, and p_r=*c*cotφ; M_f is the potential failure stress ratio; $\varphi(\ln p)$ is the curve of isotropic consolidation; $\psi(\ln\overline{p})$ is the curve of critical state; κ is the slope of rebound curve in the ε_v-ln*p* plane.

The potential failure stress ratio M_f can be written as

$$M_f=M+(R-1)(M-M_h) \tag{9}$$

where M_h is the slope of Hvorslev envelope in the *p*-*q* plane; R is the consolidation parameter and $R=\frac{\overline{p}+p_r}{p+p_r}$.

Based on the classical plastic theory (Zheng *et al*. 2002), the stress-strain relationship is expressed as follows

$$\{d\sigma\}=[D]^{ep}\{d\varepsilon\} \tag{10}$$

$$[D]^{ep}=[D]^{e}-\frac{[D]^{e}\left\{\frac{\partial g}{\partial\sigma}\right\}\left\{\frac{\partial f}{\partial\sigma}\right\}^{\mathrm{T}}[D]^{e}}{A+\left\{\frac{\partial f}{\partial\sigma}\right\}^{\mathrm{T}}[D]^{e}\left\{\frac{\partial g}{\partial\sigma}\right\}}=[D]^{e}-[D]^{p} \tag{11}$$

where $[D]^{ep}$ is the elastic-plastic constitutive matrix; $[D]^{e}$ is the elastic constitutive matrix; $[D]^{p}$ is the plastic constitutive matrix; A is the function of hardening parameter;g is the plastic potential function, and $g=f$.

Substituting Eqs. (7), (8), (9), (11) into (10), the whole process of elastic-plastic stress-strain relationship can be

calculated.

2.4 Finite element equations

It is impossible to obtain analytical solution for the deformation problem. According to the algorithm of variable stiffness in finite element method (Xie *et al*. 1981, Meng 1985), the finite elements of computational domain can be divided into three kinds of element, namely elastic elements, plastic elements and transitional elements. Therefore, the following FE formulae are obtained.

$$[K]\{\Delta\delta\} = \{\Delta R\} \tag{12}$$

$$[K] = \int_{V^e} [B]^{\mathrm{T}} [D]^e [B] dV + \int_{V^p} [B]^{\mathrm{T}} [D]^p [B] dV + \int_{V^g} [B]^{\mathrm{T}} [D]^g [B] dV \tag{13}$$

where $[K]$ is the stiffness matrix; $\{\Delta R\}$ is the increment of equivalent nodal forces vector. $[B]$ is the element strain matrix; $[D]^g$ is the transitional matrix.

Based on the algorithm of variable stiffness (Meng 1985), the transitional matrix can be written as

$$[D]^g = \bar{m}[D]^e + (1-\bar{m})[D]^p \tag{14}$$

$$\bar{m} = \frac{\Delta\bar{\sigma}_A}{\Delta\bar{\sigma}_B} \tag{15}$$

where $\bar{m}$ is the weighting coefficient; $\Delta\bar{\sigma}_A$ is the increment of equivalent stress when the finite element reaches its yield. $\Delta\bar{\sigma}_B$ is the increment of equivalent stress caused by load step.

Both [*K*] and {Δ*R*} are deterministic variables in the conventional deterministic finite element analysis, so {Δ*δ*} of Eq. (12) is a deterministic result. In this paper, [*K*] are not deterministic because the temperature and parameters are stochastic. Therefore, {Δ*δ*} of Eq. (12) is a random result.

3. Stochastic analysis methods of uncertain displacement characteristics

3.1 Random fields for soil properties

Based on the random field theory (Vanmarcke 1977 and 1983), we consider the spatial variability of mechanics properties and model the cohesion, angle of internal friction and poisson ratio as 2D random fields. When the 2D random field is divided by triangular elements (Wang *et al*. 2014), the local average random field of an element is defined as

$$X_e = \frac{1}{A_e}\int_{\Omega_e} X(x,y)dxdy \tag{16}$$

where A_e is the area of *e* and Ω_e is the possessive section of *e*.

The covariance of two local average elements is

$$Cov(X_e, X_{e'}) = \sigma^2 \sum_{K=1}^{\bar{M}} \sum_{R=1}^{\bar{M}} \omega^{(K)} \omega'^{(R)} \bar{g}(N_i^{(K)}, N_j^{(K)}, N_k^{(K)}, N_i'^{(R)}, N_j'^{(R)}, N_k'^{(R)}) \tag{17}$$

Table 1 Calculating parameter of Eq. (17)

M	1	2	3	4	5	6	7
$\omega^{(K)}$($\omega'^{(R)}$)	1/20	1/20	1/20	2/15	2/15	2/15	9/20
$N_i^{(K)}$($N_i'^{(R)}$)	1	0	0	0	1/2	1/2	1/3
$N_j^{(K)}$($N_j'^{(R)}$)	0	1	0	1/2	0	1/2	1/3
$N_k^{(K)}$($N_k'^{(R)}$)	0	0	1	1/2	1/2	0	1/3

where N_i, N_j and N_k are the shape functions of three nodes of element *e*, respectively; N_i', N_j' and N_k' are the shape functions of three nodes of element *e'*, respectively; $\bar{M}$ is the number of basis points; $\omega^{(K)}$ is the weighted coefficient of *e* and $\omega'^{(R)}$ is the weighted coefficient of *e'*.

Eq. (17) is the calculating formula of the covariance for two local average elements. In order to guarantee the calculation accuracy, we assume that $\bar{M} = 7$, and Table 1 is the calculating parameter of Eq. (17). Because the mechanical properties of frozen soil are closely connected with temperature, its strength and deformation will change greatly with minor temperature variations. The relationship will be discussed in more detail later.

3.2 NSFEM of random displacement fields

Because the covariance matrices obtained from Eq. (17) are full-rank matrices, calculating the covariance matrices is inefficient. Therefore, a set of uncorrelated random variables is obtained by orthogonal transformation method in this paper (Wang and Zhou 2013). After taking the randomness of temperature and parameters into account, the random displacement fields of an embankment can be obtained by Neumann expansion method (Yamazaki *et al*. 1988). According to Eq. (12), the following formulas can be obtained

$$\begin{cases} \{\Delta\delta\} = \{\Delta\delta\}^{(0)} - \{\Delta\delta\}^{(1)} + \{\Delta\delta\}^{(2)} - \{\Delta\delta\}^{(3)} + \mathrm{L} \\ \{\Delta\delta\}^{(0)} = [K_0]^{-1}\{\Delta R\} \\ \{\Delta\delta\}^{(m)} = [K_0]^{-1}[\Delta K]\{\Delta\delta\}^{(m\text{-}1)} \quad (m = 1,2,\mathrm{L}) \end{cases} \tag{18}$$

where $[K_0]$ is the mean of stiffness matrix, [Δ*K*] is the undulatory section.

Based on probabilistic analysis approach, the mean and standard deviation of random displacement fields can be obtained, and the computational formulas are

$$E(\boldsymbol{\delta}) = \frac{1}{N}\sum_{i=1}^{N} \boldsymbol{\delta}_i \tag{19}$$

$$S(\boldsymbol{\delta}) = \sqrt{\frac{1}{N\text{-}1}\sum_{i=1}^{N}[\boldsymbol{\delta}_i - E(\boldsymbol{\delta})]^2} = \sqrt{\frac{1}{N\text{-}1}\sum_{i=1}^{N}[\boldsymbol{\delta}_i]^2 - \frac{N}{N\text{-}1}[E(\boldsymbol{\delta})]^2} \tag{20}$$

We have made a stochastic finite element program based on aforementioned procedure, which can consider the randomness of temperature and parameters.

4. Numerical model, parameters, and boundary conditions

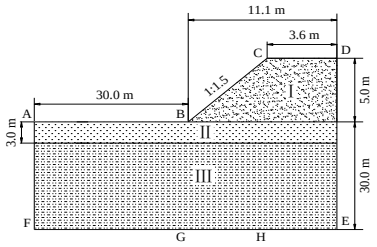

Fig. 1 The computational model. Part I is fill; Part II is silty clay and part III is weathered mudstone. (Wang *et al.* 2015)

Table 2 Basic mechanical parameters of media in embankment

Physical parameters	γ (kN·m^{-3})	a_1 (MPa)	b_1	a_2	b_2	a_3	b_3
Fill	20	0.03	0.094	23	9.5	0.35	-0.007
Silty clay	19.6	0.15	0.090	22	8	0.40	-0.008
Weathered mudstone	20.7	0.10	0.240	28	11	0.25	-0.004

Table 3 Test parameters of media in embankment

Physical parameters	κ	M_h	a	b	m	n
Fill	5.07×10^{-7}	1.06	2.12×10^-5	0.70	1.79×10^-4	0.64
Silty clay	5.12×10^{-7}	1.24	2.28×10^-5	0.72	1.88×10^-4	0.69
Weathered mudstone	5.23×10^{-7}	1.35	2.42×10^-5	0.74	1.96×10^-4	0.73

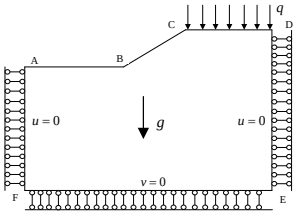

Fig. 2 Load and boundary conditions.

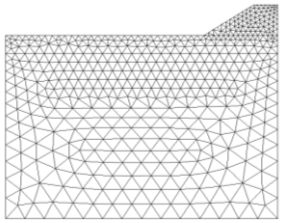

Fig. 3 Finite element meshes and random field meshes (Wang *et al.* 2015)

Table 4 Different coefficient of variation of mechanical parameters

Case	Coefficient of variation								
	c	φ	v	κ	M_h	a	b	m	n
1	0.1	0.1	0.1	0.1	0.1	0.1	0.1	0.1	0.1
2	0.25	0.25	0.25	0.25	0.25	0.25	0.25	0.25	0.25
3	0.3	0.3	0.3	0.3	0.3	0.3	0.3	0.3	0.3

Table 5 Relevant distance of mechanical parameters

Case	Vertical direction (m)	Horizontal direction (m)
1	5.0	5.0

Table 5 Continued

Case	Vertical direction (m)	Horizontal direction (m)
2	5.0	5.0
3	1.0	2.0

A typical embankment section of Qinghai-Tibet Railway is taken as a computational model and the cross section of the embankment is shown in Fig. 1. In the embankment model (Fig. 1), part I is fill, part II is silty clay and part III is weathered mudstone. The strength and deformation characteristics of embankment in permafrost regions will change greatly with small temperature variations because the mechanical properties of frozen soil are closely connected with temperature. Many literatures show that some mechanical parameters of frozen soil are determined by the following formulae (Wu *et al.* 1988, Li 2009).

$$\begin{cases} c_T = a_1 + b_1 |T| \\ \varphi_T = a_2 + b_2 |T| \\ v_T = a_3 + b_3 |T| \end{cases} \tag{21}$$

where c_T is the cohesive strength; φ_T is the angle of internal friction; v_T is the Poisson ratio; $a_i(i=1,2,3)$ and $b_i(i=1,2,3)$ are the experimental coefficients. Their values of experimental clay are given in Table 2. If the soil temperature is greater than 0 °C, $b_i(i=1,2,3)$ is equal to 0. T is the soil temperature.

According to the test results of triaxial compression (Lai *et al*. 2009 and 2010), the curve of isotropic consolidation $\varphi(\ln p)$ and the curve of critical state $\psi(\ln \bar{p})$ can be approximated by the following formulae

$$\begin{cases} \varphi(\ln p) = a e^{b \ln p} \\ \psi(\ln \bar{p}) = m e^{n \ln \bar{p}} \end{cases} \tag{22}$$

where a, b, m and n are the experimental coefficients. Their values of experimental clay are given in Table 3.

According to Chinese code for design on railway subgrade (Railway Ministry of PRC 2005), Qinghai-Tibet Railway belongs to II-level railway whose design speed is 80 km/h≤v≤120 km/h, and its conversion load is uniform load whose intensity is 60.1kPa and width is 3.5 m. Fig. 2 is the load and boundary conditions. In detail, the x direction and y direction of the native surfaces (AB, BC, CD) are free; the x direction of the lateral boundaries (AF, DE) are constrained while the y direction of the lateral boundaries are free; the x direction of the bottom boundaries (EF) are free while the y direction of the bottom boundaries are constrained.

Both the structure and the random fields were discretized into triangle elements. The finite element meshes and random field meshes is shown in Fig. 3. It can be seen that the random field mesh is same with the finite element mesh, and they are the same with the discrete mesh of thermal analysis (Wang *et al*. 2015), which greatly reduces the programming work. We assumed that the embankment is completed on 15 July and the experimental coefficients of isotropic consolidation curve and critical state curve follow normally distributed random variable.

The cohesion, angle of internal friction and poisson ratio for the fill and silty clay are taken as three independent random fields. Considering three cases where the coefficients of variation are 0.1, 0.25 and 0.3. According to the research of Zhu and Zhang (2013), we assumed the correlation length is 5m in both horizontal and vertical direction for case 1 and case 2. The relevant distance is 1m in vertical direction, and the value of horizontal direction is 20 m for case 3. Tables 4 and 5 are the details.

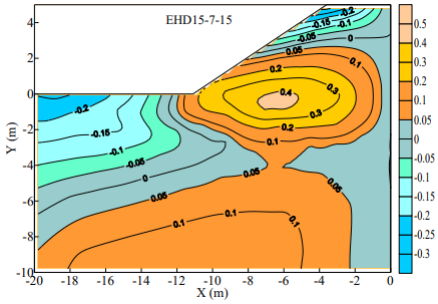

(a)

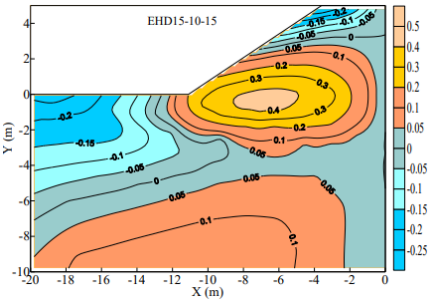

(b)

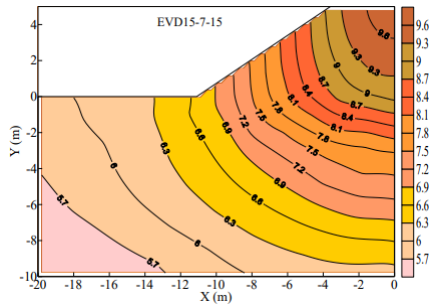

(c)

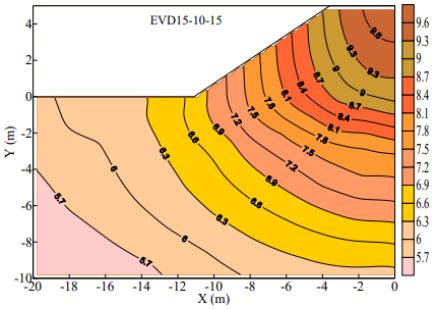

(d)

Fig. 4. Distributions of mean displacement for the 15th year after construction (Unit: cm). (a) lateral mean displacement on July 15, (b) lateral mean displacement on October 15, (c) vertical mean displacement on July 15 and (d) vertical mean displacement on October 15

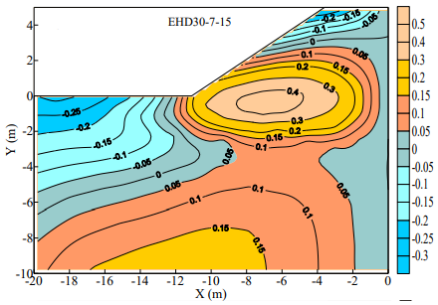

(a)

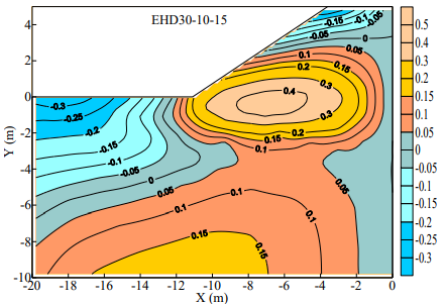

(b)

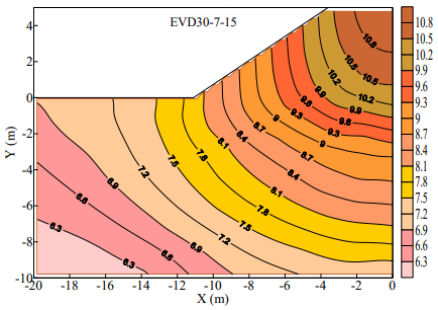

(c)

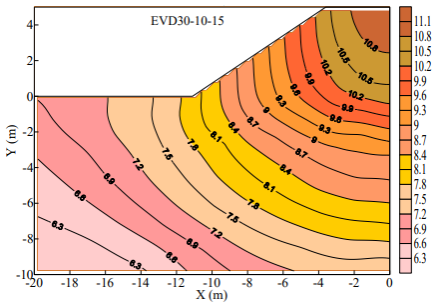

(d)

Fig. 5 Distributions of mean displacement for the 30th year after construction (Unit: cm). (a) lateral mean displacement on July 15, (b) lateral mean displacement on October 15, (c) vertical mean displacement on July 15 and (d) vertical mean displacement on October 15

5. Results and analyses

In order to correspond to the results of random temperature field (Wang *et al.* 2015), we choose and analyze the stochastic displacement fields for some specific time, which are July 15 and October 15 in the 15th and 30th year.

5.1 Results and analyses for the mean displacement

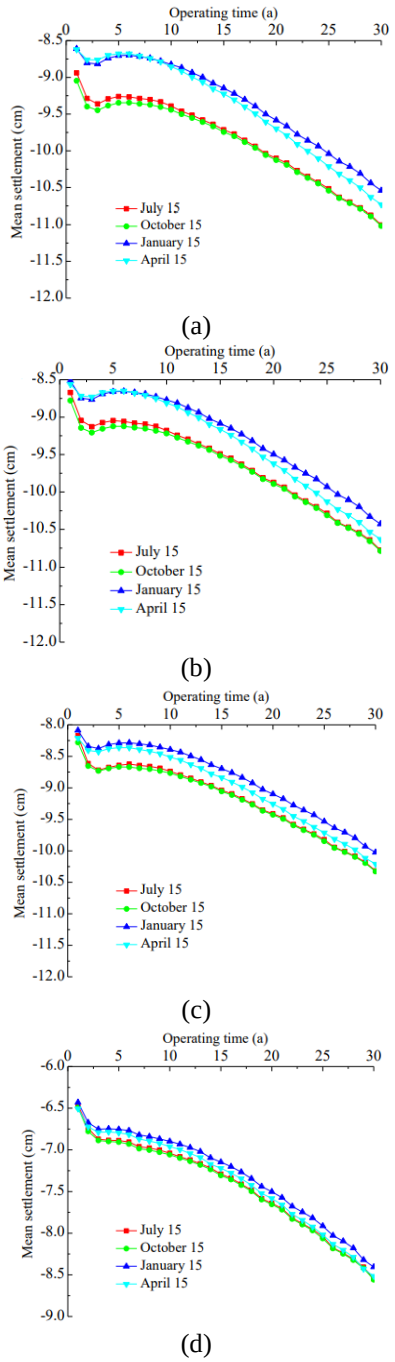

Fig. 6 Mean settlement curves of characteristic points, (a) Top central point, (b) 2 m under the top central point, (c) 5 m under the top central point and (d) 10 m under the top central point

Fig. 4 shows the distribution of lateral mean displacement and vertical mean displacement on July 15 and October 15 after 15 years of the construction, respectively. From Figs. 4(a) and 4(b), we can see that the lateral mean displacement is smaller and the maximum is 0.45 cm and 0.46 cm on July 15 and October 15. Figs. 4(c) and 4(d) show that the vertical mean displacement is bigger and the maximum is 9.71cm and 9.73 cm on July 15 and October 15. Fig. 5 shows the distribution of lateral mean displacement and vertical mean displacement on July 15 and October 15 after 30 years of the construction, and the

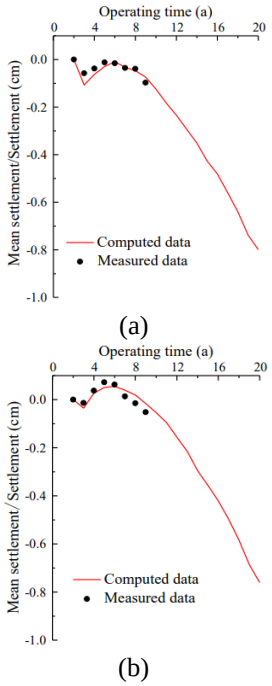

Fig. 7 Comparisons between the measured and computed settlement at the positions, (a) Top central point and (b) Left shoulder point

maximum is 0.47 cm, 0.48 cm, 11.1 cm and 11.2 cm, respectively. Comparing Figs. 4(a), 4(b), 5(a) and 5(b), we can find that the distributions of lateral mean displacement are exactly similar. Therefore, we can conclude that the change of random temperature fields have little influence on lateral mean displacement. Comparing Figs. 4(c), 4(d), 5(c) and 5(d), we can find that the distributions of vertical mean displacement are different for different years, and the mean in the 30th is bigger than the mean in the 15th because of the climatic warming. Therefore, we can conclude that the change of random temperature fields has a relatively greater impact on vertical mean displacement and the climatic warming will lead to its increase.

Fig. 6 shows the mean settlement of characteristic points, which are the top central point (No. D, Fig. 1), 2 m under the top central point, 5m under the top central point and 10 m under the top central point. From Fig. 6(a), we can see that there are three stages for the mean settlement curves of the top central point on July 15, October 15, January 15 and April 15. From the 1st year to the 3rd year after construction, the mean settlement is very evident because the construction of embankment will lead to widespread melting of permafrost. From the 3rd year to the 6th year after construction, the mean settlement value is positive because the new embankment is refreezing and some thawed soils develop into frozen soils. After 7 years of the construction, the mean settlement will increase year by year because the climatic warming accelerates the degradation of permafrost. For Figs. 6(b) and 6(c), a similar conclusion can be made. In Fig. 6(d), the three stages aren't obvious because the effect from construction disturbance is small. Based on the measured date (Ma *et al.* 2011, Mu 2012), Fig. 7(a) presents the measured and computed settlement with respect to time at the top central point on July 15 after 2 years of the construction. Fig. 7(b) presents

the measured and computed settlement with respect to time at the left shoulder point on January 15 after 2 years of the construction. It is observed that the mean settlement is roughly same between statistical measured date and computed date. Therefore, according to the law of large numbers of Bernoulli, the stochastic analytical model can describe the uncertain displacement characteristics for embankment in permafrost regions.

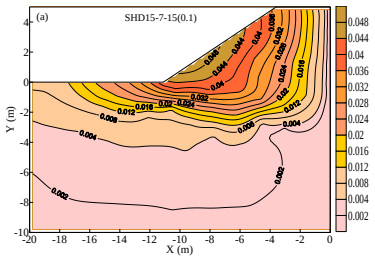

(a)

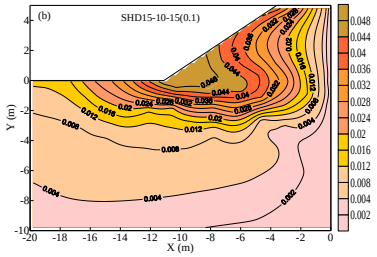

(b)

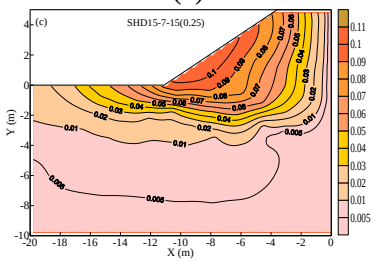

(c)

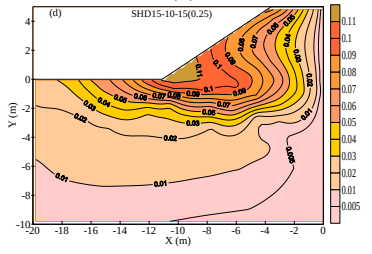

(d)

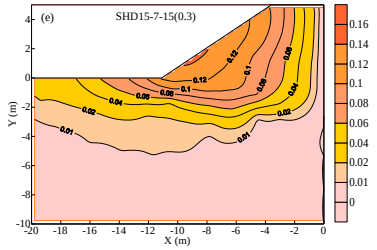

(e)

Fig. 8 Distributions of standard deviation of lateral displacement for the 15th year after construction (Unit: cm). (a) on July 15, case 1, (b) on October 15, case 1, (c) on July 15, case 2, (d) on October 15, case 2, (e) on July 15, case 3 and (f) on October 15, case 3

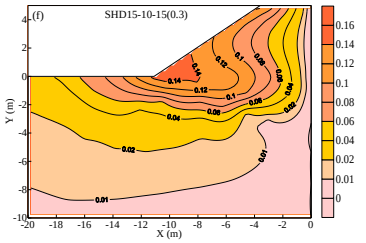

(f)

Fig. 8 Continued

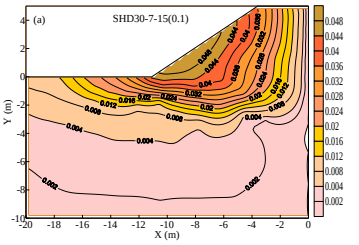

(a)

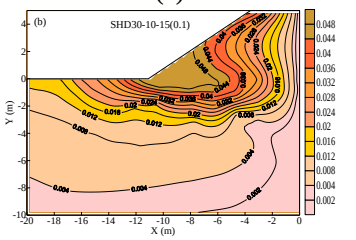

(b)

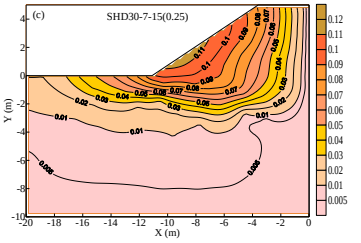

(c)

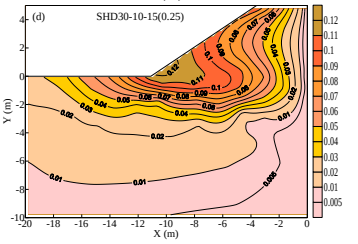

(d)

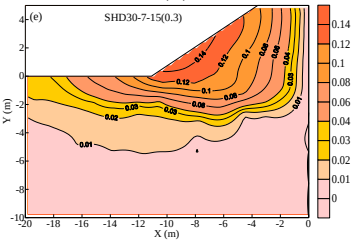

(e)

Fig. 9 Distributions of standard deviation of lateral displacement for the 30th year after construction (Unit: cm). (a) on July 15, case 1, (b) on October 15, case 1, (c) on July 15, case 2, (d) on October 15, case 2, (e) on July 15, case 3 and (f) on October 15, case 3

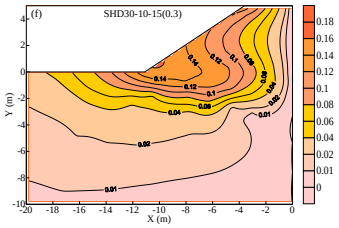

(f)

Fig. 9 Continued

5.2 Results and analyses for the standard deviation

Figs. 8 and 9 show the distribution of standard deviations of lateral displacement on July 15 and October 15 in the 15th and 30th year, respectively. From Figs. 8(a), 8(b), 9(a) and 9(b), we can see that the standard deviations of lateral displacement are smaller and the maximum is about 0.05cm. When the coefficients of variation are 0.25, Figs. 8(c), 8(d), 9(c) and 9(d) show that the standard deviations of lateral displacement are bigger and the maximum is about 0.13 cm. When the coefficients of variation are 0.3, Figs. 8(e), 8(f), 9(e) and 9(f) show that the maximum for the standard deviations of lateral displacement is about 0.16 cm. Comparing Figs. 8(a), 8(c) and 8(e), 8(b), 8(d) and 8(f), 9(a), 9(c) and 9(e), 9(b), 9(d) and 9(f), the standard deviations is bigger for same locations when the coefficients of variation are 0.25 and 0.3, therefore, we can conclude that, for the same time and same locations, the bigger the coefficients of variation are, the bigger the standard deviations are. Comparing Figs. 8(a), 8(b), 9(a) and 9(b), we can find that the distributions of standard deviation of lateral displacement are exactly similar. Therefore, we can conclude that the change of random temperature fields have little influence on standard deviation of lateral displacement. For Figs. 8(c), 8(d), 9(c) and 9(d), a similar conclusion can be made. Figs.10 and 11 show the distribution of standard deviations of vertical displacement on July 15 and October 15 in the 15th and

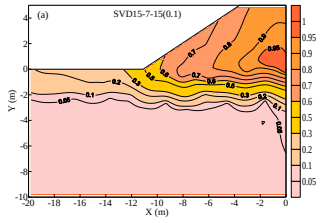

(a)

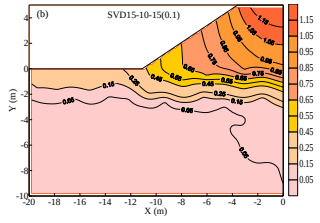

(b)

Fig. 10 Distributions of standard deviation of vertical displacement for the 15th year after construction (Unit: cm). (a) on July 15, case 1, (b) on October 15, case 1, (c) on July 15, case 2, (d) on October 15, case 2, (e) on July 15, case 3 and (f) on October 15, case 3

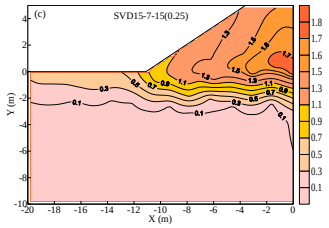

(c)

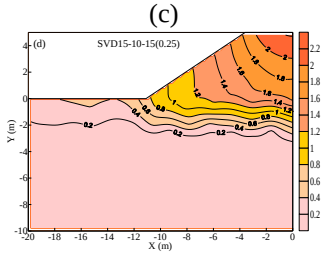

(d)

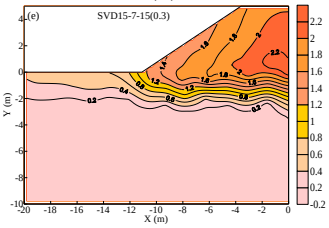

(e)

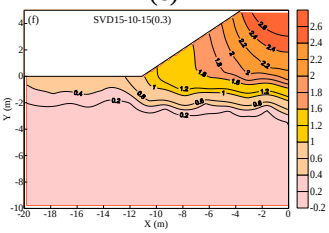

(f)

Fig. 10 Distributions of standard deviation of vertical displacement for the 15th year after construction (Unit: cm). (a) on July 15, case 1, (b) on October 15, case 1, (c) on July 15, case 2, (d) on October 15, case 2, (e) on July 15, case 3 and (f) on October 15, case 3

30th year, respectively. Figs. 10(a) and 10(b), 11(a) and 11(b) show that the larger standard deviation on July 15 is at the bottom of the fill while the larger standard deviation on October 15 is at the surface of the fill. It means that the random temperature fields have a great influence on the distribution of standard deviations of vertical displacement. Comparing Figs. 10(a) and 11(a), 10(b) and 11(b), we can see that the standard deviations in the 30th are bigger than the standard deviations in the 15th because of the climatic warming.

In order to evaluate the change of standard deviation for the settlement characteristic, Figs. 12, 13 and 14 show the standard deviations of characteristic points, which are the top central point, 2m under the top central point, 5m under the top central point and 10m under the top central point for case 1, case 2 and case 3, respectively. It can be found from Fig. 12(a)-12(c) that the standard deviation on July 15, October 15, January 15 and April 15 increases with time. From the 1st year to the 15th years after construction, the standard deviation will be increasing very fast because

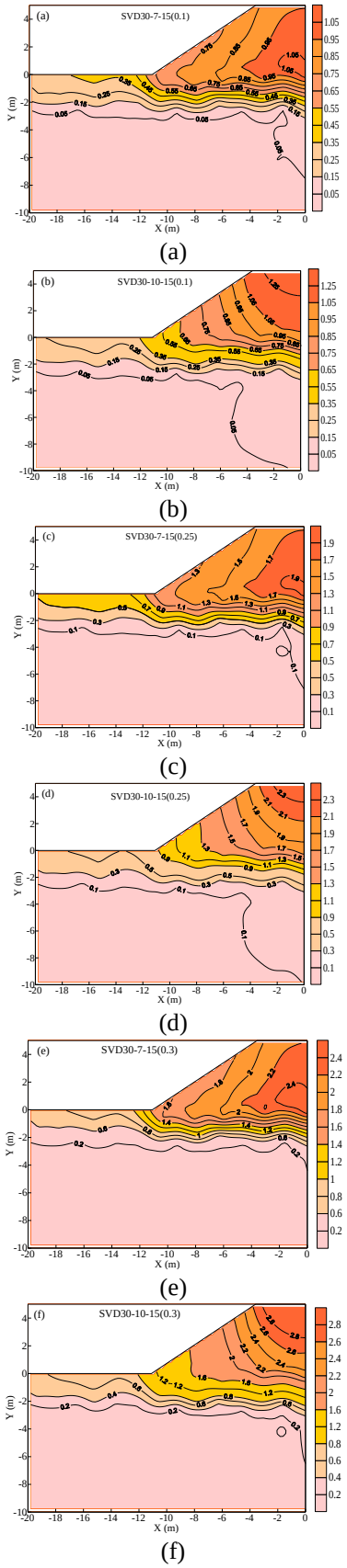

Fig. 11 Distributions of standard deviation of vertical displacement for the 30th year after construction (Unit: cm). (a) on July 15, case 1, (b) on October 15, case 1, (c) on July 15, case 2, (d) on October 15, case 2, (e) on July 15, case 3 and (f) on October 15, case 3

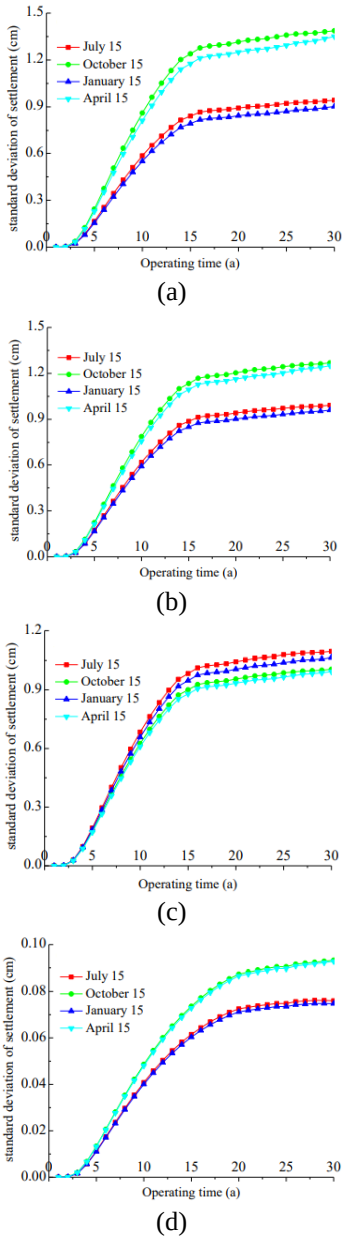

Fig. 12 Standard deviation of settlement curves of characteristic points for case 1, (a) Top central point, (b) 2 m under the top central point, (c) 5 m under the top central point and (d) 10 m under the top central point

the temperature field of the embankment is unstable. Both the climate warming and the construction disturbance have an effect on the results. After the 15th years, the standard deviation will be increasing very slowly because the effect of construction disturbance is disappeared. Only the climate warming has an effect on the results. For Figs. 12(d), the change of standard deviation is continuous because the deeper of location is, the smaller of construction disturbance is. From Figs. 13(a)-13(d) and 14(a)-14(d), a similar conclusion can be made. Therefore, we can conclude that, with the passage of time, the settlement characteristic of conventional deterministic analysis may be farther from the true value. It is necessary to take the stochastic aspects of the temperature and parameters into account for engineering design.

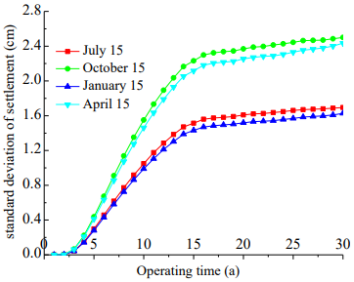

(a)

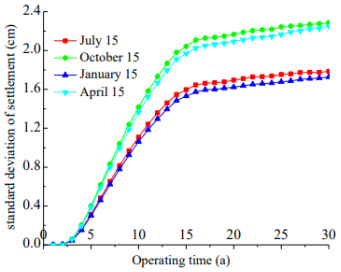

(b)

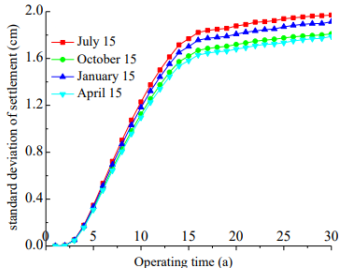

(c)

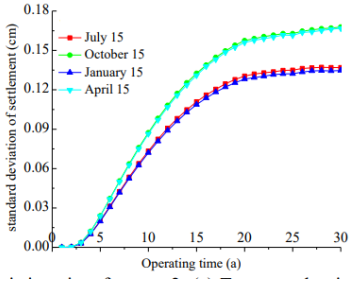

(d)

Fig. 13 Standard deviation of settlement curves of characteristic points for case 2, (a) Top central point, (b) 2 m under the top central point, (c) 5 m under the top central point and (d) 10 m under the top central point

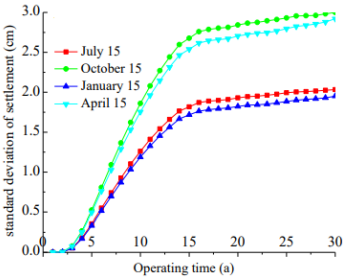

(a)

Fig. 14 Standard deviation of settlement curves of characteristic points for case 3, (a) Top central point, (b) 2 m under the top central point, (c) 5 m under the top central point and (d) 10 m under the top central point

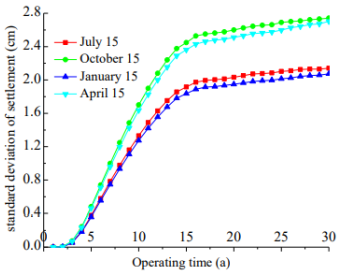

(b)

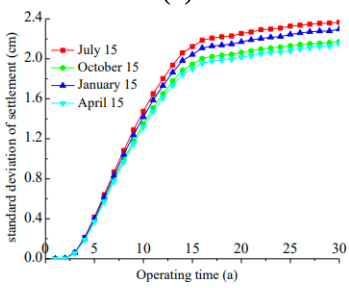

(c)

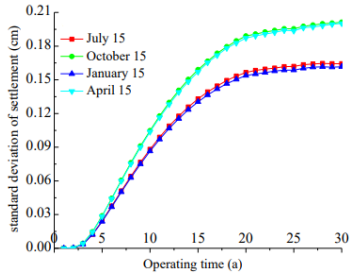

(d)

Fig. 14 Continued

5. Conclusions

In this paper, the stochastic deformation fields of foundations in permafrost regions are investigated by probabilistic analysis approach. In view of the randomness of temperature and parameters, we mode the mechanics properties as random fields and consider the influence of random temperature on the basic mechanical parameters of frozen soil. A stochastic coupling program is compiled by MATLAB, and the mean and standard deviation of uncertain deformation characteristics for an embankment in a permafrost region are obtained by NSFEM. According to this study, the following conclusions can be drawn:

• The change of stochastic temperature has little influence on the mean and standard deviation of lateral displacement while it has a relatively greater impact on the mean and standard deviation of vertical displacement. There are three stages for the mean settlement of characteristic points due to the effect of construction disturbance and climate warming.

• When the coefficients of variation are different, the distributions of mean displacement are the same and the distributions of standard deviation are similar for the three cases. For the same time and same locations, the bigger the coefficients of variation are, the bigger the standard deviations are.

• Considering the stochastic effect of temperature and parameters, the standard deviation of settlement increases

with time. Therefore, with the passage of time, the settlement characteristic of conventional deterministic analysis may be farther from the true value.

At present, there are few theoretical documents on the uncertain deformation characteristics of foundations in permafrost regions because it involves multi-disciplinary knowledge and is difficult to be described by a universal theory. In this paper, although stochastic temperature and parameters are taken into account in the stochastic analysis model and there is much progress compared with previous studies on random temperature fields (Liu *et al*. 2014, Wang *et al*. 2015), some issues remain to be discussed. For example, the moisture, heat and stress in permafrost regions have an interaction process; the stochastic analysis model does not consider the moisture migration problems. Our stochastic coupling program needs to be optimized because it is inefficient. In addition, we make some assumptions for the stochastic mechanics parameters because there are not actual statistical data in this paper. Notwithstanding these limitations, as a preliminary study, it is expected to provide theoretical basis and reference for foundation engineering in permafrost regions.

Acknowledgements

The authors wish to express their thanks to the very competent Reviewers for the valuable comments and suggestions. This research was supported by the National Natural Science Foundation of China (Grant No.51604265) and the China Postdoctoral Science Foundation funded project (Grant No.2017M620229).

References

Dasaka, S.M. and Zhang, L.M. (2012), "Spatial variability of in situ weathered soil", *Geotechnique*, **62**(5), 375-384.

Davis, R.O. and Selvadurai, A.P.S. (2002), *Plasticity and Geotechnics*, Cambridge University Press, Cambridge, U.K.

Elkateb, T., Chalaturnyk, R. and Robertson, P.K. (2003), "An overview of soil heterogeneity: Quantification and implications on geotechnical field problems", *Can. Geotech. J.*, **40**(1), 1-15.

Fattah, M.Y., Zabar, B.S. and Hassan, H.A. (2015), "Soil arching analysis in embankments on soft clays reinforced by stone columns", *Struct. Eng. Mech.*, **56**(4), 507-534.

Khemis, A., Chaouche, A.H., Athmani, A. and Kong, F.T. (2016), "Uncertainty effects of soil and structural properties on the buckling of flexible pipes shallowly buried in Winkler foundation", *Struct. Eng. Mech.*, **59**(4), 739-759.

Lai, Y.M., Li, S.Y., Qi, J.L., Gao, Z.H. and Chang, X.X. (2008), "Strength distributions of warm frozen clay and its stochastic damage constitutive model", *Cold Reg. Sci. Technol.*, **53**(2), 200-215.

Lai, Y.M., Jin, L. and Chang, X.X. (2009), "Yield criterion and elasto-plastic damage constitutive model for frozen sandy soil", *J. Plastic.*, **25**(6), 1177-1205.

Lai, Y.M., Yang, Y.G., Chang, X.X. and Li, S.Y. (2010), "Strength criterion and elastoplastic constitutive model of frozen silt in generalized plastic mechanics", *J. Plastic.*, **26**(10), 1461-1484.

Lai, Y.M., Li, J.B. and Li, Q.Z. (2012), "Study on damage statistical constitutive model and stochastic simulation for warm ice-rich frozen silt", *Cold Reg. Sci. Technol.*, **71**(2), 102-110.

Lee, J., Jeong, S. and Lee, J.K. (2015). "3D analytical method for mat foundations considering coupled soil springs", *Geomech. Eng.*, **8**(6), 845-857.

Li, N., Xu, B. and Chen, F.X. (2006), "Coupling analysis of temperature, deformation and stress field for frozen soil roadbed", *Chin. J. Highway Transport*, **19**(3), 1-7 (in Chinese).

Li, S.Y., Lai, Y.M., Zhang, M.Y. and Dong Y. H. (2009), "Study on long-term stability Qinghai-Tibet Railway embankment", *Cold Reg. Sci. Technol.*, **57**(2-3), 139-147.

Liu, Y.Z., Wu, Q.B., Zhang, J.M. and Yu, S. (2002), "Deformation of highway roadbed in permafrost regions of the Tibetan Plateau", *J. Glaciol. Geocryol.*, **24** (1), 10-15 (in Chinese).

Liu, Z.Q., Lai, Y.M., Zhang, X.F. and Zhang, M.Y. (2006), "Random temperature fields of embankment in cold regions", *Cold Reg. Sci. Technol.*, **45**(2), 76-82.

Liu, Z.Q., Lai, Y.M., Zhang, M.Y. and Zhang, X.F. (2007), "Numerical analysis for random temperature fields of embankment in cold regions", *Sci. Chin. Series D Earth Sci.*, **50**(3), 404-410.

Liu, Z.Q., Yang, W.H. and Wei, J. (2014), "Analysis of random temperature field for freeway with wide subgrade in cold regions", *Cold Reg. Sci. Technol.*, **106**, 22-27

Ma, W. and Wang, D.Y. (2014), *Mechanics of Frozen Soil*, China Science Press, Beijing, China.

Ma, W., Mu, Y.H., Wu, Q.B., Sun, Z.Z. and Liu, Y.Z. (2011), "Characteristics and mechanisms of embankment deformation along the Qinghai-Tibet Railway in permafrost regions", *Cold Reg. Sci. Technol.*, **67**(3), 178-186

Mao, X.S.,Wang, B.G., Hu, C.S. and Dou M.J. (2006), "Numerical analyses of deformation and stress fields in permafrost regions", *J. Glaciol. Geocryol.*, **28**(3), 396-400 (in Chinese).

Meng, F.Z. (1985), *Thoery of Elasto-Plastic Finite Deformation and Finite Element Method*, Tsinghua University Press, Beijing, China.

Mu, Y.H. (2012), "Analyses on dynamic variations of embankment thermal regime and deformation along the Qinghai-Tibet railway in permafrost regions", Ph.D. Dissertation, Graduate University of Chinese Academy of Sciences, Lanzhou, China.

Parinaz, J. and Ehsan, J. (2016), "Reliability sensitivities with fuzzy random uncertainties using genetic algorithm", *Struct. Eng. Mech.*, **60**(3), 413-431.

Sun, Z.K., Wang, L.J., Bai, M.Z. and Wei, Q. C. (2003), "Study on deformation feature of railway embankment in permafrost regions on Tibet Plateau", *Chin. Safety Sci. J.*, **13**(8), 25-28.

TB 10001 (2005), *Code for Design on Subgrade of Railway*, Railway Ministry of PRC, Beijing, China.

Vanmarcke, E.H. (1977), "Probabilistic modeling of soil profiles", *J. Geotech. Eng. Div.*, **103**(11), 1227-1246.

Vanmarcke, E. (1983), *Random Fields: Analysis and Synthesis*, MIT Press, Cambridge, U.K.

Wang, C., Zhou, S., Wang, B., Guo, P. and Su, H. (2015). "Differential settlements in foundations under embankment load: Theoretical model and experimental verification", *Geomech. Eng.*, **8**(2), 283-303.

Wang, S.J., Huang, X.M. and Hou, S.G. (2006), "Numerical analyses of pavement deformation and stress in permafrost regions", *J. Glaciol. Geocryol.*, **28**(2), 217-222 (in Chinese).

Wang, S.H., Qi, J.L., Yu, F. and Liu, F.Y. (2016), "A novel modeling of settlement of foundations in permafrost regions", *Geomech. Eng.*, **10**(2), 225-245.

Wang, T. and Zhou, G.Q. (2013), "Neumann stochastic finite element method for calculating temperature field of frozen soil based on random field theory", *Sci. Cold Arid Reg.*, **5**(4), 488-497.

Wang, T., Zhou, G.Q., Yin, Q.Y. and Xia, L.J. (2014), "Local average method of triangular elements for discretization of the random filed of geotechnical parameters", *Rock Soil Mech.*,

35(5), 1482-1488 (in Chinese).

Wang, T., Zhou, G.Q., Wang, J.Z., Zhao, X.D., Yin, Q.Y., Xia, L.J. and Liu, Y.Y. (2015), "Stochastic analysis model of uncertain temperature characteristics for embankment in warm permafrost regions", *Cold Reg. Sci. Technol.*, **109**, 43-52.

Wang, T. (2015), "Study on the analysis model of stochastic temperature fields and displacement fields in permafrost regions", Ph.D. Dissertation, China University of Mining and Technology, Xuzhou. China

Wu, Z.W., Cheng, G.D. and Zhu, L.N. (1988), *Roadbed Engineering in Permafrost Region*, Lanzhou University Press, Lanzhou, China.

Xie, Y.Q. and He, F.B. (1981), *The Finite Element Method in Elastic and Plastic Mechanic*, China Machine Press, Beijing, China.

Yamazaki, F., Shinozuka, M. and Dasgupta, G. (1988), "Neumann expansion for stochastic finite element analysis", *J. Eng. Mech.*, **114**(8), 1335-1354.

Yao, Y.P., Zhou, A.N. and Lu, D.C. (2007), "Extended transformed stress space for geomaterials and its application", *J. Eng. Mech.*, **133**(10), 1115-1123.

Yao, Y.P., Sun, D.A. and Matsuoka, H. (2008), "A unified constitutive model for both clay and sand with hardening parameter independent on stress path", *Comput. Geotech.*, **35**(2) 210-222.

Yao, Y.P. and Kong, Y.X. (2012), "Extended UH model: Three-dimensional unified hardening model for anisotropic clays", *J. Eng. Mech.*, **138**(7), 853-866.

Yu, Q.H., Liu, Y.Z. and Tong, C.J. (2002), "Analysis of the subgrade deformation of the Qinghai-Tibetan highway", *J. Glaciol. Geocryol.*, **24**(5), 623-627 (in Chinese).

Zheng, Y., Shen, Z. and Gong, X. (2002), *Generalized Plastic Mechanics-The Principles of Geotechnical Plastic Mechanics*, China Architecture and Building Press, Beijing, China.

Zhou, G.Q., Wang, T., Wang, J.Z. and Zhao, X.D. (2015), "Stochastic analysis of uncertain temperature characteristics for expressway with wide subgrade in cold regions", *Cold Reg. Sci. Technol.*, **114**, 36-43.

Zhu, H. and Zhang, L.M. (2013), "Characterizing geotechnical anisotropic spatial variations using random field theory", *Can. Geotech. J.*, **50**(7), 723-734.

CC